Bulk Photovoltaic Effect Driven by Collective Excitations in a Correlated Insulator

Tatsuya Kaneko,[1] Zhiyuan Sun,[1] Yuta Murakami,[2] Denis Golež,[3,4,5] and Andrew J. Millis[1,3]
[1]Department of Physics, Columbia University, New York, New York 10027, USA
[2]Department of Physics, Tokyo Institute of Technology, Meguro, Tokyo 152-8551, Japan
[3]Center for Computational Quantum Physics, Flatiron Institute, New York, New York 10010, USA
[4]Faculty of Mathematics and Physics, University of Ljubljana, Jadranska 19, SI-1000 Ljubljana, Slovenia
[5]Jozef Stefan Institute, Jamova 39, SI-1000 Ljubljana, Slovenia

(Received 17 December 2020; accepted 10 August 2021; published 17 September 2021)

We investigate the bulk photovoltaic effect, which rectifies light into electric current, in a collective quantum state with correlation driven electronic ferroelectricity. We show via explicit real-time dynamical calculations that the effect of the applied electric field on the electronic order parameter leads to a strong enhancement of the bulk photovoltaic effect relative to the values obtained in a conventional insulator. The enhancements include both resonant enhancements at sub-band-gap frequencies, arising from excitation of optically active collective modes, and broadband enhancements arising from nonresonant deformations of the electronic order. The deformable electronic order parameter produces an injection current contribution to the bulk photovoltaic effect that is entirely absent in a rigid-band approximation to a time-reversal symmetric material. Our findings establish that correlation effects can lead to the bulk photovoltaic effect and demonstrate that the collective behavior of ordered states can yield large nonlinear optical responses.

DOI: 10.1103/PhysRevLett.127.127402

The photovoltaic effect is the optical process that converts light into electrical current [1–3]. Photovoltaic effects can be obtained from devices with interfaces (e.g., *p-n* junctions), but potential applications to new types of solar cells have driven recent interest in bulk photovoltaic effects (BPVE) occurring in homogeneous noncentrosymmetric materials, where artificially fabricated interfaces are not required and a photovoltage is not limited by a band gap energy [4–8].

The BPVE has been extensively analyzed in ferroelectrics [9–15] and Weyl semimetals [16–19]. Theory distinguishes shift and injection current contributions to the BPVE, generated by photoinduced changes in the electron position and velocity, respectively [3,19]. The shift current contribution in ferroelectrics and Weyl semimetals has been related to Berry connection and topological effects [19–22]. The fundamental assumption underlying this previous work is that the BPVE may be studied in a model of independent electrons moving in a rigid band structure. This assumption has important consequences. For example, while an injection current contribution has the potential to lead to large nonlinear conductivity [8], the independent particle approximation predicts that the injection current under linearly polarized light vanishes in time-reversal-symmetric insulators [3,19].

In this Letter, we show that electronic correlation effects can substantially enhance the BPVE, opening a new pathway to the design of optoelectronic materials. The crucial new point is that if the inversion symmetry breaking arises from a low energy electronic instability, then in addition to resonant enhancements at electronic collective mode frequencies, an applied electric field can nonresonantly deform the electronic band structure in ways that activate an injection current contribution.

We investigate the effect theoretically in the context of the excitonic insulator (EI) but we emphasize that our generic results apply to any inversion-symmetry breaking collective electronic states. Recently proposed EI candidate materials include $TiSe_2$ [23–26], Ta_2NiSe_5 [27–32], and WTe_2 [33–35]. The EI state is characterized by spontaneous band hybridization triggered by the interband Coulomb interaction in narrow-gap semiconductors and semimetals [36–41]. The excitonic order may break inversion symmetry, leading to "electronic ferroelectricity" [42–45], in which case the state is referred to as a ferroelectric EI (FEI). In this Letter, we investigate the BPVE in a FEI. We compute the optical response including changes in the order parameter, identify the optically active collective modes in the FEI, and demonstrate that nonlinear excitation leads not only to resonant enhancement of the shift current but also to a nonvanishing injection current with both resonant and broadband contributions. The nonvanishing injection current contribution means that in contrast to simple band insulators the FEI can exhibit large nonlinear conductivity.

A minimal theoretical model of the FEI [Fig. 1(a)] is

$$\begin{aligned}\hat{\mathcal{H}} = &-t_a\sum_j(\hat{c}^\dagger_{j+1,a}\hat{c}_{j,a}+\text{H.c.})-t_b\sum_j(\hat{c}^\dagger_{j+1,b}\hat{c}_{j,b}+\text{H.c.})\\ &-t_{ab}\sum_j(\hat{c}^\dagger_{j,a}\hat{c}_{j,b}+\text{H.c.})+t_{ab}\sum_j(\hat{c}^\dagger_{j,a}\hat{c}_{j-1,b}+\text{H.c.})\\ &+D\sum_j(\hat{n}_{j,a}-\hat{n}_{j,b})+V\sum_j\hat{n}_{j,a}(\hat{n}_{j,b}+\hat{n}_{j-1,b}),\end{aligned}\quad(1)$$

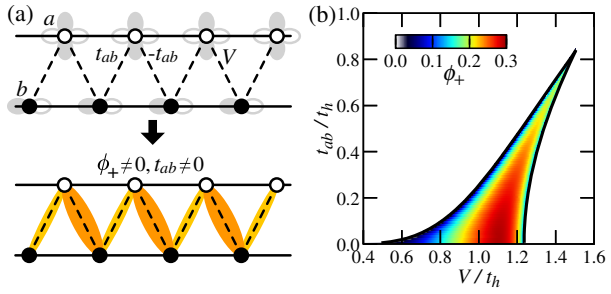

FIG. 1. (a) Top panel: Zigzag chain model Eq. (1), where we plot an example of two orbitals that lead to hopping t_{ab}. Bottom panel: schematic picture of the EI state. (b) Ground-state phase diagram of Eq. (1) in the plane of interaction V and interchain hopping t_{ab} computed in the Hartree-Fock approximation for $D/t_h = 1$. The magnitude of the order parameter ϕ_+ is shown in false color.

where $\hat{c}_{j,\alpha}$ ($\hat{c}^\dagger_{j,\alpha}$) is the annihilation (creation) operator of a fermion on the chain (orbital) $\alpha(=a,b)$ at site j, and $\hat{n}_{j,\alpha} = \hat{c}^\dagger_{j,\alpha}\hat{c}_{j,\alpha}$. t_α is the hopping integral on the chain α, and t_{ab} is the interchain hopping that has the opposite signs along the $+x$ and $-x$ directions. This type of hopping appears when two orbitals have opposite parities along the chain direction [see, e.g., Fig. 1(a)] [46,47]. D is the energy level difference, and V is the interchain Coulomb interaction that induces the excitonic instability. For simplicity, we take a particle-hole symmetric band structure with $t_a = -t_b = t_h$ but our results do not depend in any important way on this assumption. We focus on the half-filled case $\langle \hat{n}_{j,a}\rangle + \langle \hat{n}_{j,b}\rangle = 1$ and set t_h (t_h^{-1}) as a unit of energy (time) [48].

Excitonic order in Eq. (1) is characterized by the expectation values $\phi(x/2) = \langle \hat{c}^\dagger_{j,a}\hat{c}_{j,b}\rangle$ and $\phi(-x/2) = \langle \hat{c}^\dagger_{j,a}\hat{c}_{j-1,b}\rangle$ which it is convenient to combine into the even and odd parity hybridizations $\phi_\pm = \phi(x/2) \pm \phi(-x/2)$. For later use, we also define $\Delta n = \langle \hat{n}_{j,b}\rangle - \langle \hat{n}_{j,a}\rangle$. At $t_{ab} = 0$, the number of particles on each chain is separately conserved and the model has an associated internal $U(1)$ invariance which is spontaneously broken in the EI state, leading to an one-parameter family of degenerate EI states characterized by $\phi_+ = |\phi_+|e^{i\theta_+} \neq 0$ with $\phi_- = 0$. The collective mode associated with variation of the $U(1)$ phase θ_+ is gapless [49,50]. When $t_{ab} \neq 0$, the $U(1)$ symmetry is reduced to Z_2, $\phi_- \neq 0$ and is real at all temperatures, and the excitonic order is characterized by the appearance of a nonvanishing ϕ_+ with the phase $\theta_+ = 0$, π, which spontaneously breaks the Z_2 symmetry. Because the broken symmetry is discrete, all collective modes are gapped. The association of the EI transition with a discrete symmetry breaking is generic in materials [47,50–52]; in the EI case considered here the Z_2 breaking also makes the $+x$ and $-x$ direction hybridization magnitude different, thereby breaking inversion symmetry [see Fig. 1(a)]. Following the modern theory of polarization [53–55], we find the polarization $P = \int (dk/2\pi)\mathcal{A}_{--}(k) \propto V\phi_+ t_{ab}$, where $\mathcal{A}_{--}(k)$ is the Berry connection at momentum k in the occupied band [56], confirming that when $\phi_+ \neq 0$ and $t_{ab} \neq 0$ the Z_2-broken phase of Eq. (1) is a correlation-driven ferroelectric.

We solve the model in the time-dependent mean-field (tdMF) theory which captures both the symmetries of the ground state and the needed properties of the collective modes and nonlinear response [66–69]. The ground state calculation is standard [56] and the resulting phase diagram is shown in Fig. 1(b). The dynamics are most conveniently studied in a pseudospin representation $\rho_\nu(k,t) \equiv \langle \hat{\Psi}_k(t)^\dagger \sigma_\nu \hat{\Psi}_k(t)\rangle/2$ (σ_ν: Pauli matrix) with $\hat{\Psi}^\dagger_k = [\hat{c}^\dagger_{k,a}, \hat{c}^\dagger_{k,b}]$. We use the equation of motion (EOM) in the length gauge [3,56]

$$\frac{\partial}{\partial t}\boldsymbol{\rho}(k,t) = 2\boldsymbol{h}(k,t)\times\boldsymbol{\rho}(k,t) - E(t)\frac{\partial}{\partial k}\boldsymbol{\rho}(k,t) - \gamma[\boldsymbol{\rho}(k,t) - \boldsymbol{\rho}_{\rm eq}(k)], \tag{2}$$

where $\boldsymbol{h}(k,t)$ is the tdMF Hamiltonian in the pseudospin representation:

$$\begin{aligned} h_x(k,t) &= -V\mathrm{Re}[\phi_+(t)]\cos\frac{k}{2} - V\mathrm{Im}[\phi_-(t)]\sin\frac{k}{2}, \\ h_y(k,t) &= (2t_{ab} + V\mathrm{Re}[\phi_-(t)])\sin\frac{k}{2} - V\mathrm{Im}[\phi_+(t)]\cos\frac{k}{2}, \\ h_z(k,t) &= -2t_h\cos k + D + V\Delta n(t). \end{aligned} \tag{3}$$

Here, we introduce a phenomenological relaxation term γ which may be thought of as the scattering of photo-excited carriers by phonons, disorders, and many-body effects [70–74]. At each point in time, the MF parameters are instantaneously updated using the equations $\phi_\pm(t) = 2\int(dk/2\pi)[\rho_x(k,t) + i\rho_y(k,t)]\Lambda_\pm(k)$ [where $\Lambda_+(k) = \cos(k/2)$ and $\Lambda_-(k) = i\sin(k/2)$] and $\Delta n(t) = -2\int(dk/2\pi)\rho_z(k,t)$. We solve the equations numerically for a continuous-wave field $E(t) = E_0\sin\omega_p t$ and initial condition $\boldsymbol{\rho}(k,t=0) = \boldsymbol{\rho}_{\rm eq}(k)$ [56].

Figure 2(a) shows the optical conductivity $\sigma_{xx}(\omega)$ defined here as the Fourier coefficient $J(\omega = \omega_p)$ of the (total) current $J(t) = 2\int(dk/2\pi)[\partial_k \boldsymbol{h}(k,t)]\cdot\boldsymbol{\rho}(k,t)$ at steady state ($t \gg \gamma^{-1}$). In the FEI, $\sigma_{xx}(\omega)$ exhibits two peaks below the band gap, arising from the collective modes of the ordered state. The collective modes are optically active because for $t_{ab} \neq 0$ the ground state breaks inversion symmetry. The reduction of the $U(1)$ symmetry down to Z_2 by $t_{ab} \neq 0$ means that the two modes are each gapped even at longest wavelength. They have mixed phase and amplitude character, but the lower (upper) mode is of dominantly phase (amplitude) mode character. As can be seen from Fig. 2(b), when the system is excited at the frequency of the lower peak, the imaginary part of $\phi_+(t)$ oscillates more strongly than the real part. On the other

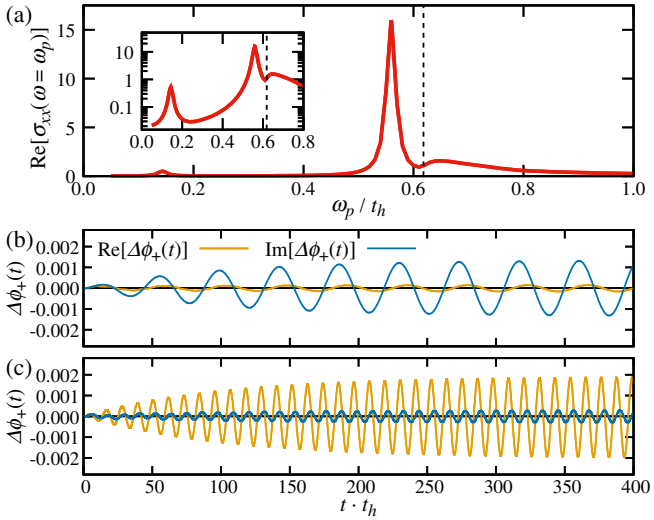

FIG. 2. (a) Optical conductivity $\sigma_{xx}(\omega=\omega_p)$ of the FEI on linear (main panel) and logarithmic (inset) scales. The black dashed line indicates the band gap. (b),(c) Time evolution of the real (orange) and imaginary (blue) components of the order parameter $\phi_+(t)$ at (b) $\omega_p/t_h=0.144$ and (c) $\omega_p/t_h=0.559$, which correspond to the phase and amplitude mode frequencies, respectively, where $\Delta\phi_+(t)=\phi_+(t)-\phi_+(t=0)$ is plotted. $D/t_h=1$, $t_{ab}/t_h=0.2$, $V/t_h=1.1$, $E_0/t_h=0.0001$, and $\gamma/t_h=0.01$ are used.

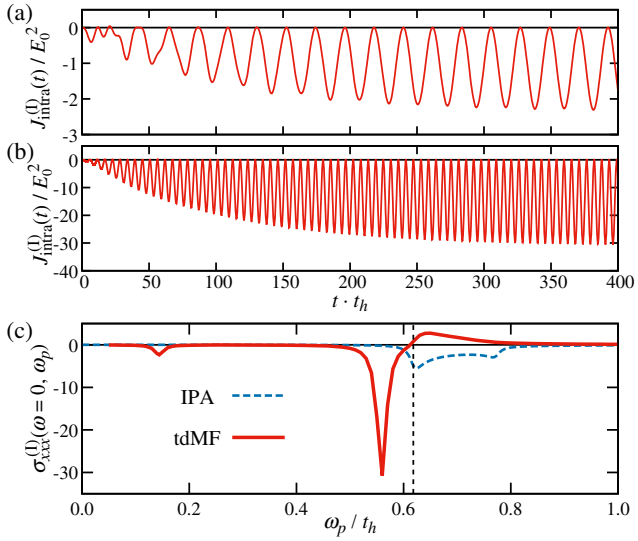

FIG. 3. (a),(b) Time evolution of the intraband current $J^{(\mathrm{I})}_{\mathrm{intra}}(t)$ in the FEI at (a) $\omega_p/t_h=0.144$ and (b) $\omega_p/t_h=0.559$, which correspond to the collective mode frequencies in Figs. 2(b) and 2(c), respectively. (c) Conductivity $\sigma^{(\mathrm{I})}_{xxx}(\omega=0;\omega_p)$ of the shift current. The red solid and blue dashed lines indicate $\sigma^{(\mathrm{I})}_{xxx}(\omega=0;\omega_p)$ in the tdMF and IPA, respectively. The parameter set is the same as Fig. 2.

hand, when the system is excited at the frequency of the upper peak, the real part of $\phi_+(t)$ strongly oscillates [see Fig. 2(c)]. Note that the upper peak is separated from the continuum because the band gap including the interchain hopping t_{ab} is larger than the gap originated from $V\phi_+$. Since these two modes are optically active, their contributions to higher-order optical responses are important.

We now discuss the BPVE, which we define as the dc limit of the intraband current J_{intra} produced by an applied ac electric field. We derive J_{intra} from the time derivative of intraband polarization P_{intra} [3]. Details are given in the Supplemental Material [56]. We find

$$J_{\mathrm{intra}}(t)=\int\frac{dk}{2\pi}\mathrm{tr}[\mathcal{J}(k,t)\tilde{\rho}(k,t)], \tag{4}$$

where $\mathcal{J}$ is defined below and the density matrix $\tilde{\rho}(k,t)$ is obtained via EOM (2), which comprises $\tilde{\rho}(k,t)=\tilde{\rho}_{\mathrm{eq}}(k)+\tilde{\rho}^{(1)}(k,t)+\tilde{\rho}^{(2)}(k,t)+\cdots$ [superscript indicates order in powers of $E(t)$]. The BPVE is second order in E and following prior work we distinguish shift and injection current contributions which are most conveniently written in the band basis (labeled here by n, m) of instantaneous eigenstates of $\boldsymbol{h}(k,t)$ in Eq. (3) [where $\tilde{\rho}(k,t)$ is defined in the band basis].

The shift current contribution arises from the generalized derivative $r_{nm;k}(k)=\partial_k\mathcal{A}_{nm}(k)-i[\mathcal{A}_{nn}(k)-\mathcal{A}_{mm}(k)]\mathcal{A}_{nm}(k)$ $(n\neq m)$, which gives the shift vector related to polarization described by the Berry connection [3,21], where $\mathcal{A}_{nm}(k)=i\boldsymbol{U}^\dagger_n(k)\partial_k\boldsymbol{U}_m(k)$ is defined by the eigenvector $\boldsymbol{U}_n(k)$ of the band $\varepsilon_n(k)$. $\mathcal{J}$ of the shift current is given by

$$\mathcal{J}^{(\mathrm{I})}_{nm}(k,t)=-E(t)r_{nm;k}(k,t). \tag{5}$$

Because $\mathcal{J}^{(\mathrm{I})}\propto E(t)$, the density matrix of first order $\tilde{\rho}^{(1)}(k,t)$ contributes to shift current generation. Figures 3(a) and 3(b) show $J^{(\mathrm{I})}_{\mathrm{intra}}(t)=\int(dk/2\pi)\mathrm{tr}[\mathcal{J}^{(\mathrm{I})}(k,t)\tilde{\rho}(k,t)]$ computed for applied electric field equal to the collective mode frequencies. We see immediately that while $J^{(\mathrm{I})}_{\mathrm{intra}}(t)$ oscillates, there is a nonzero average, which increases smoothly from zero and saturates, implying a dc photocurrent in the long-time limit. Since the BPVE is characterized by $J(\omega=0)=2\sigma_{xxx}(\omega=0;\omega_p)|E(\omega_p)|^2$, it is useful to present the results in terms of the nonlinear conductivity $\sigma_{xxx}(\omega=0;\omega_p)$ defined as $(2/E_0^2T_p)\int_{t_m}^{t_m+T_p}J(t)dt$, where $T_p=2\pi/\omega_p$ and t_m $(\gg\gamma^{-1})$ is a time long enough for steady state to be reached [56]. Figure 3(c) shows $\sigma^{(\mathrm{I})}_{xxx}(\omega=0;\omega_p)$ corresponding to our results for $J^{(\mathrm{I})}_{\mathrm{intra}}(t)$. Corresponding to Figs. 3(a) and 3(b), $\sigma^{(\mathrm{I})}_{xxx}(0;\omega_p)$ in the tdMF shows two sharp peaks in the sub-band-gap regime, indicating that excitation of collective modes (especially the amplitudelike mode) makes a large contribution to the shift current.

For comparison, we also plot in Fig. 3(c) $\sigma^{(\mathrm{I})}_{xxx}(0;\omega_p)$ obtained from the independent particle approximation (IPA) that assumes that the MF parameter magnitude and phase remain fixed during the excitation process. We see that in the IPA the conductivity is nonzero only in the above-band-gap regime and is smaller in magnitude than the amplitude mode contribution, showing that the collective dynamics of the electronically ordered state make a large contribution to the nonlinear conductivity.

Next, we examine the injection current contribution [3], for which

$$\mathcal{J}^{(\mathrm{II})}_{nm}(k,t) = v_n(k,t)\delta_{nm}, \tag{6}$$

where $v_n(k,t) = \partial_k \varepsilon_n(k,t)$. Because $\mathcal{J}^{(\mathrm{II})}$ does not contain $E(t)$, the density matrix of second order $\tilde{\rho}^{(2)}(k,t)$ contributes to injection current generation. Figure 4(a) shows the injection current contribution to the BPVE for different values of the phenomenological relaxation γ. When $\gamma \neq 0$, $J^{(\mathrm{II})}_{\mathrm{intra}}(t)$ increases linearly at short times and saturates for times $\gg \gamma^{-1}$, which is a characteristic of the injection current [8,75]. Our result for the FEI is contrasted to the IPA result that for a free system with time-reversal symmetry linearly polarized light does not produce an injection current. In Fig. 4(b), we plot the nonlinear conductivity $\sigma^{(\mathrm{II})}_{xxx}(\omega = 0;\omega_p)$ corresponding to $J^{(\mathrm{II})}_{\mathrm{intra}}(t)$, which exhibits two sharp peaks at the sub-band-gap collective mode frequencies and in addition the large broadband contribution in the above-band-gap regime. Since the injection current is of order γ^{-1} [8,56], it can correspond to a strong optical response when dissipative effects are small. As shown in Fig. 5, the conductivity $\sigma^{(\mathrm{I})}_{xxx}(0;\omega_p) + \sigma^{(\mathrm{II})}_{xxx}(0;\omega_p)$ exhibits large values with increasing γ^{-1} due to the injection current contribution.

Finally, we show how the injection current arises from photoinduced deformations of the order parameter (see the Supplemental Material [56] for details). In the velocity gauge [75,76], the injection current may be written

$$\begin{aligned} J_{\mathrm{IC}}(0;\omega_p) = \int \frac{dk}{2\pi}\int \frac{d\omega'}{2\pi}\mathrm{tr}[&\mathcal{V}_0(k)G_0(k,\omega')\delta\Delta^{(1)}(k,-\omega_p) \\ &\times G_0(k,\omega'+\omega_p)\delta\Delta^{(1)}(k,\omega_p)G_0(k,\omega')] \\ &+ [\omega_p \leftrightarrow -\omega_p], \end{aligned} \tag{7}$$

where $G_0(k,\omega)$ is the bare fermion propagator and $\mathcal{V}_0(k) = t_{ab}\cos(k/2)\sigma_2 + 2t_h \sin(k)\sigma_3$ is the k derivative of the tight-binding Hamiltonian. $\delta\Delta^{(1)}(k,\omega_p)$ is the perturbation at first order of $A(\omega_p) \propto E(\omega_p)/\omega_p$ (vector potential). If the MF parameters were fixed to their equilibrium values (i.e., IPA), $\delta\Delta^{(1)}(k,\omega_p) = -\mathcal{V}_0(k)A(\omega_p)$ and the injection current in Eq. (7) vanishes due to $\mathcal{V}_0(-k) = -\mathcal{V}_0(k)^*$ [56]. However, in the FEI the incident light modulates $\delta\Delta_\pm(t) = V\phi_\pm(t) - V\phi^{\mathrm{eq}}_\pm$ and $\delta n(t) = \Delta n(t) - \Delta n^{\mathrm{eq}}$ [see e.g., Fig. 2] so that the total perturbation $\delta\Delta^{(1)}(k,\omega_p) = -\mathcal{V}_0(k)A(\omega_p) + \delta\Delta^{(1)}_{\mathrm{MF}}(k,\omega_p)$ contains $\delta\Delta^{(1)}_{\mathrm{MF}}(k,\omega_p) = \delta\boldsymbol{\Delta}(k,\omega_p)\cdot\boldsymbol{\sigma}$ given by

$$\begin{aligned} \delta\Delta_x(k,\omega_p) &= -\delta\Delta^R_+(\omega_p)\cos\frac{k}{2} - \delta\Delta^I_-(\omega_p)\sin\frac{k}{2}, \\ \delta\Delta_y(k,\omega_p) &= -\delta\Delta^I_+(\omega_p)\cos\frac{k}{2} + \delta\Delta^R_-(\omega_p)\sin\frac{k}{2}, \\ \delta\Delta_z(k,\omega_p) &= V\delta n(\omega_p), \end{aligned} \tag{8}$$

where the superscripts R and I indicate the real and imaginary part of the order parameter, respectively. The inversion-breaking nature of the FEI phase means $\delta\Delta_\pm(\omega_p) \propto A(\omega_p)$ and $\delta\Delta^{(1)}(-k,-\omega_p) \neq -\delta\Delta^{(1)}(k,\omega_p)^*$, which makes a nonvanishing contribution to the integrands in Eq. (7). Hence, order parameter deformations produce a nonvanishing injection current.

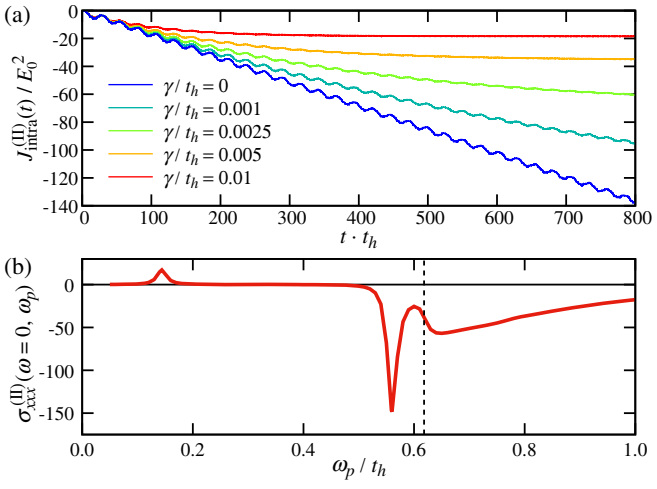

FIG. 4. (a) Time evolution of the intraband current $J^{(\mathrm{II})}_{\mathrm{intra}}(t)$ in the FEI at $\omega_p/t_h = 0.8$. (b) Conductivity $\sigma^{(\mathrm{II})}_{xxx}(\omega = 0;\omega_p)$ of the injection current with $\gamma/t_h = 0.01$. $D/t_h = 1$, $t_{ab}/t_h = 0.2$, $V/t_h = 1.1$, and $E_0/t_h = 0.0001$ are used.

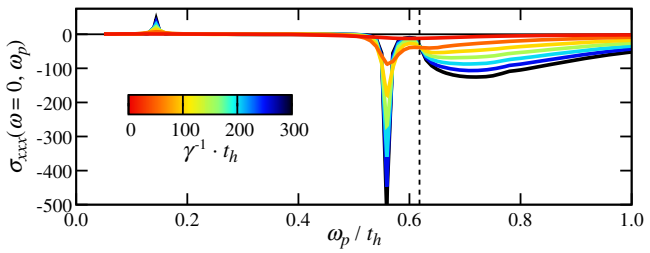

FIG. 5. Conductivity $\sigma_{xxx}(\omega = 0;\omega_p) = \sigma^{(\mathrm{I})}_{xxx}(\omega = 0;\omega_p) + \sigma^{(\mathrm{II})}_{xxx}(\omega = 0;\omega_p)$ with changing γ. The parameter set is the same as Fig. 4.

In summary, we have investigated the shift and injection current contributions to the BPVE in a correlated inversion-symmetry-breaking insulator: the FEI. The physics of the correlated insulator produces characteristic enhancements of the BPVE, related to the deformability of the order parameter under applied electric fields. The shift current is modified and shows sharp resonances at the collective mode frequencies. The injection current has both resonant contributions at the collective mode frequencies and a broadband contribution at above-band-gap drive frequencies which arises from the deformability of the order parameter and is entirely absent in a rigid band picture. It is very weak in the phonon-driven ferroelectric case because the energy scale mismatch between the phonon frequency and electronic band gap weakens the influence of the phonon motion on the electronic system [56].

In contrast to the previous studies that address excitonic effects [74,77–79], we focus on collective order-parameter dynamics in a symmetry-broken state and reveal its effects on the BPVE. While we used a simple one-dimensional model of a FEI, our idea is applicable to higher dimensions and richer models. The essential ingredient is a deformable electronic order parameter that produces a broken symmetry. Although our two-chain model is similar to models proposed for Ta_2NiSe_5 [47], in Ta_2NiSe_5 the ordered state is inversion symmetric and the BPVE vanishes. However, under an applied bias voltage, Ta_2NiSe_5 has shown the light-intensity-dependent photocurrent generation [80]. The mechanism of current generation under both dc and optical electric fields is an interesting open question. The FEI has recently been predicted in the monolayer transition metal dichalcogenides [81], which is a potential candidate that exhibits the BPVE. The search for materials candidates should include the properties (a) inversion-symmetry breaking (e.g., the ferroelectric state) and (b) strong electronic character of the order.

This work was supported by Grants-in-Aid for Scientific Research from JSPS, KAKENHI Grants No. JP18K13509 (T. K.), No. JP19K23425, No. JP20K14412, No. JP20H05265 (Y. M.) and JST CREST Grant No. JPMJCR1901 (Y. M.). A. J. M. and Z. S. acknowledge support from the Energy Frontier Research Center on Programmable Quantum Materials funded by the U.S. Department of Energy (DOE), Office of Science, Basic Energy Sciences (BES), under Award No. DE-SC0019443. The numerical calculations were performed in part using computational resources at RIKEN. T. K. was supported by the JSPS Overseas Research Fellowship. D. G. is supported by Slovenian Research Agency (ARRS) under Program J1-2455 and P1-0044. The Flatiron Institute is a division of the Simons Foundation.

[1] V. I. Belinicher and B. I. Sturman, Sov. Phys. Usp. **23**, 199 (1980).
[2] R. von Baltz and W. Kraut, Phys. Rev. B **23**, 5590 (1981).
[3] J. E. Sipe and A. I. Shkrebtii, Phys. Rev. B **61**, 5337 (2000).
[4] L. Z. Tan, F. Zheng, S. M. Young, F. Wang, S. Liu, and A. M. Rappe, npj Comput. Mater. **2**, 16026 (2016).
[5] J. E. Spanier, V. M. Fridkin, A. M. Rappe, A. R. Akbashev, A. Polemi, Y. Qi, Z. Gu, S. M. Young, C. J. Hawley, D. Imbrenda, G. Xiao, A. L. Bennett-Jackson, and C. L. Johnson, Nat. Photonics **10**, 611 (2016).
[6] A. M. Cook, B. M. Fregoso, F. de Juan, S. Coh, and J. E. Moore, Nat. Commun. **8**, 14176 (2017).
[7] T. Rangel, B. M. Fregoso, B. S. Mendoza, T. Morimoto, J. E. Moore, and J. B. Neaton, Phys. Rev. Lett. **119**, 067402 (2017).
[8] Y. Zhang, T. Holder, H. Ishizuka, F. de Juan, N. Nagaosa, C. Felser, and B. Yan, Nat. Commun. **10**, 3783 (2019).
[9] W. Koch, R. Munser, W. Ruppel, and P. Würfel, Solid State Commun. **17**, 847 (1975).
[10] S. M. Young and A. M. Rappe, Phys. Rev. Lett. **109**, 116601 (2012).
[11] T. Choi, S. Lee, Y. J. Choi, V. Kiryukhin, and S.-W. Cheong, Science **324**, 63 (2009).
[12] S. M. Young, F. Zheng, and A. M. Rappe, Phys. Rev. Lett. **109**, 236601 (2012).
[13] M. Nakamura, S. Horiuchi, F. Kagawa, N. Ogawa, T. Kurumaji, Y. Tokura, and M. Kawasaki, Nat. Commun. **8**, 281 (2017).
[14] N. Ogawa, M. Sotome, Y. Kaneko, M. Ogino, and Y. Tokura, Phys. Rev. B **96**, 241203(R) (2017).
[15] M. Sotome, M. Nakamura, J. Fujioka, M. Ogino, Y. Kaneko, T. Morimoto, Y. Zhang, M. Kawasaki, N. Nagaosa, Y. Tokura, and N. Ogawa, Proc. Natl. Acad. Sci. U.S.A. **116**, 1929 (2019).
[16] Y. Zhang, H. Ishizuka, J. van den Brink, C. Felser, B. Yan, and N. Nagaosa, Phys. Rev. B **97**, 241118(R) (2018).
[17] J. Ma, Q. Gu, Y. Liu, J. Lai, P. Yu, X. Zhuo, Z. Liu, J.-H. Chen, J. Feng, and D. Sun, Nat. Mater. **18**, 476 (2019).
[18] G. B. Osterhoudt, L. K. Diebel, M. J. Gray, X. Yang, J. Stanco, X. Huang, B. Shen, N. Ni, P. J. W. Moll, Y. Ran, and K. S. Burch, Nat. Mater. **18**, 471 (2019).
[19] J. Ahn, G.-Y. Guo, and N. Nagaosa, Phys. Rev. X **10**, 041041 (2020).
[20] T. Morimoto and N. Nagaosa, Sci. Adv. **2**, e1501524 (2016).
[21] B. M. Fregoso, T. Morimoto, and J. E. Moore, Phys. Rev. B **96**, 075421 (2017).
[22] N. Nagaosa and T. Morimoto, Adv. Mater. **29**, 1603345 (2017).
[23] H. Cercellier, C. Monney, F. Clerc, C. Battaglia, L. Despont, M. G. Garnier, H. Beck, P. Aebi, L. Patthey, H. Berger, and L. Forró, Phys. Rev. Lett. **99**, 146403 (2007).
[24] C. Monney, H. Cercellier, F. Clerc, C. Battaglia, E. F. Schwier, C. Didiot, M. G. Garnier, H. Beck, P. Aebi, H. Berger, L. Forró, and L. Patthey, Phys. Rev. B **79**, 045116 (2009).
[25] A. Kogar, M. S. Rak, S. Vig, A. A. Husain, F. Flicker, Y. I. Joe, L. Venema, G. J. MacDougall, T. C. Chiang, E. Fradkin, J. van Wezel, and P. Abbamonte, Science **358**, 1314 (2017).
[26] T. Kaneko, Y. Ohta, and S. Yunoki, Phys. Rev. B **97**, 155131 (2018).

[27] Y. Wakisaka, T. Sudayama, K. Takubo, T. Mizokawa, M. Arita, H. Namatame, M. Taniguchi, N. Katayama, M. Nohara, and H. Takagi, Phys. Rev. Lett. **103**, 026402 (2009).

[28] T. Kaneko, T. Toriyama, T. Konishi, and Y. Ohta, Phys. Rev. B **87**, 035121 (2013); **87**, 199902(E) (2013).

[29] K. Seki, Y. Wakisaka, T. Kaneko, T. Toriyama, T. Konishi, T. Sudayama, N. L. Saini, M. Arita, H. Namatame, M. Taniguchi, N. Katayama, M. Nohara, H. Takagi, T. Mizokawa, and Y. Ohta, Phys. Rev. B **90**, 155116 (2014).

[30] Y. F. Lu, H. Kono, T. I. Larkin, A. W. Rost, T. Takayama, A. V. Boris, B. Keimer, and H. Takagi, Nat. Commun. **8**, 14408 (2017).

[31] K. Sugimoto, S. Nishimoto, T. Kaneko, and Y. Ohta, Phys. Rev. Lett. **120**, 247602 (2018).

[32] K. Matsubayashi *et al.*, J. Phys. Soc. Jpn. **90**, 074706 (2021).

[33] P. Wang, G. Yu, Y. Jia, M. Onyszczak, F. A. Cevallos, S. Lei, S. Klemenz, K. Watanabe, T. Taniguchi, R. J. Cava, L. M. Schoop, and S. Wu, Nature (London) **589**, 225 (2021).

[34] P. A. Lee, Phys. Rev. B **103**, L041101 (2021).

[35] Y. Jia *et al.*, arXiv:2010.05390.

[36] L. V. Keldysh and Y. V. Kopeav, Fiz. Tverd. Tela **6**, 2791 (1964) [Sov. Phys. Solid State **6**, 2219 (1965)].

[37] D. Jérome, T. M. Rice, and W. Kohn, Phys. Rev. **158**, 462 (1967).

[38] B. I. Halperin and T. M. Rice, Rev. Mod. Phys. **40**, 755 (1968).

[39] P. B. Littlewood, P. R. Eastham, J. M. J. Keeling, F. M. Marchetti, B. D. Simons, and M. H. Szymanska, J. Phys. Condens. Matter **16**, S3597 (2004).

[40] F. X. Bronold and H. Fehske, Phys. Rev. B **74**, 165107 (2006).

[41] J. Kuneš, J. Phys. Condens. Matter **27**, 333201 (2015).

[42] E. Batyev and V. Borisyuk, Zh. Eksp. Teor. Fiz. **32**, 419 (1980) [JETP Lett. **32**, 395 (1980)], http://jetpletters.ru/ps/1428/article_21726.shtml.

[43] T. Portengen, T. Östreich, and L. J. Sham, Phys. Rev. B **54**, 17452 (1996).

[44] C. D. Batista, Phys. Rev. Lett. **89**, 166403 (2002).

[45] Z. Sun, T. Kaneko, D. Golež, and A. J. Millis, Phys. Rev. Lett. **127**, 127702 (2021).

[46] T. Sandu, Phys. Rev. B **72**, 125105 (2005).

[47] G. Mazza, M. Rösner, L. Windgätter, S. Latini, H. Hübener, A. J. Millis, A. Rubio, and A. Georges, Phys. Rev. Lett. **124**, 197601 (2020).

[48] The light velocity (c), the charge (q), the Planck constant ($\hbar$), and the lattice constant (a) are set to 1. In Figs. 3–5, $\sigma_{xxx}(\omega = 0; \omega_p)$ $[J_{\text{intra}}(t)/E_0^2]$ is plotted in units of $q^3a^2/\hbar t_h \propto t_h^{-1}$.

[49] Z. Sun and A. J. Millis, Phys. Rev. B **102**, 041110(R) (2020).

[50] Y. Murakami, D. Golež, T. Kaneko, A. Koga, A. J. Millis, and P. Werner, Phys. Rev. B **101**, 195118 (2020).

[51] B. Zenker, H. Fehske, and H. Beck, Phys. Rev. B **90**, 195118 (2014).

[52] T. Kaneko, B. Zenker, H. Fehske, and Y. Ohta, Phys. Rev. B **92**, 115106 (2015).

[53] R. D. King-Smith and D. Vanderbilt, Phys. Rev. B **47**, 1651 (1993).

[54] D. Vanderbilt and R. D. King-Smith, Phys. Rev. B **48**, 4442 (1993).

[55] R. Resta, Rev. Mod. Phys. **66**, 899 (1994).

[56] See Supplemental Material at http://link.aps.org/supplemental/10.1103/PhysRevLett.127.127402 for details, which includes Refs. [57–65].

[57] O. Matsyshyn, F. Piazza, R. Moessner, and I. Sodemann, arXiv:2104.00689.

[58] M. Bukov, L. D'Alessio, and A. Polkovnikov, Adv. Phys. **64**, 139 (2015).

[59] D. J. Scalapino, S. R. White, and S. C. Zhang, Phys. Rev. Lett. **68**, 2830 (1992).

[60] G. B. Ventura, D. J. Passos, J. M. B. Lopes dos Santos, J. M. Viana Parente Lopes, and N. M. R. Peres, Phys. Rev. B **96**, 035431 (2017).

[61] D. Kaplan, T. Holder, and B. Yan, Phys. Rev. Lett. **125**, 227401 (2020).

[62] A. Altland and B. D. Simons, *Condensed Matter Field Theory*, 2nd ed. (Cambridge University Press, Cambridge, England, 2010).

[63] Z. Sun, M. M. Fogler, D. N. Basov, and A. J. Millis, Phys. Rev. Research **2**, 023413 (2020).

[64] N. Tsuji and H. Aoki, Phys. Rev. B **92**, 064508 (2015).

[65] M. J. Rice and E. J. Mele, Phys. Rev. Lett. **49**, 1455 (1982).

[66] Y. Murakami, D. Golež, M. Eckstein, and P. Werner, Phys. Rev. Lett. **119**, 247601 (2017).

[67] D. Golež, Z. Sun, Y. Murakami, A. Georges, and A. J. Millis, Phys. Rev. Lett. **125**, 257601 (2020).

[68] H. M. Bretscher, P. Andrich, Y. Murakami, D. Golež, B. Remez, P. Telang, A. Singh, L. Harnagea, N. R. Cooper, A. J. Millis, P. Werner, A. K. Sood, and A. Rao, Sci. Adv. **7**, eabd6147 (2021).

[69] The tdMF calculation is essentially equivalent to the solution of the Bethe-Salpeter equation with the vertex correction.

[70] C. Attaccalite and M. Grüning, Phys. Rev. B **88**, 235113 (2013).

[71] I. Al-Naib, J. E. Sipe, and M. M. Dignam, Phys. Rev. B **90**, 245423 (2014).

[72] S. A. Mikhailov, Phys. Rev. B **93**, 085403 (2016).

[73] D. J. Passos, G. B. Ventura, J. M. Viana Parente Lopes, J. M. B. Lopes dos Santos, and N. M. R. Peres, Phys. Rev. B **97**, 235446 (2018).

[74] Y.-H. Chan, D. Y. Qiu, F. H. da Jornada, and S. G. Louie, Proc. Natl. Acad. Sci. U.S.A. **118**, e1906938118 (2021).

[75] T. Holder, D. Kaplan, and B. Yan, Phys. Rev. Research **2**, 033100 (2020).

[76] D. E. Parker, T. Morimoto, J. Orenstein, and J. E. Moore, Phys. Rev. B **99**, 045121 (2019).

[77] T. Morimoto and N. Nagaosa, Phys. Rev. B **94**, 035117 (2016).

[78] R. Fei, L. Z. Tan, and A. M. Rappe, Phys. Rev. B **101**, 045104 (2020).

[79] T. Morimoto and N. Nagaosa, Phys. Rev. B **102**, 235139 (2020).

[80] L. Li, W. Wang, L. Gan, N. Zhou, X. Zhu, Q. Zhang, H. Li, M. Tian, and T. Zhai, Adv. Funct. Mater. **26**, 8281 (2016).

[81] D. Varsano, M. Palummo, E. Molinari, and M. Rontani, Nat. Nanotechnol. **15**, 367 (2020).